npj | heritage science

Article

https://doi.org/10.1038/s40494-025-01936-z

Applications of surface adaptive micro X-ray fluorescence scanner in cultural relics

Qiong Xu[1,2], Yifan Wang[1,3], Xu Zhou[1,3], Peiquan Duan[4], Yong Liu[5], Jiangtao Gao[5], Long Wei[1,2], Cunfeng Wei[1,2] ✉ & Liang Qu[4] ✉

Micro X-ray fluorescence (μXRF) can obtain the elemental distribution in the surfaces of cultural relics and provide valuable information for archaeologists. We developed a surface adaptive μXRF scanner enabling large-area elemental imaging on cultural relics with arbitrary irregular surfaces, overcoming limitations of existing systems constrained by object shape and size. We conducted μXRF scanning on an enamel cylinder covered with paper, a fallen painting from ancient architecture and an unearthed gnomon shadow template, generating the corresponding elemental distribution images. Using the surface adaptive μXRF scanner, we successfully conducted large-area μXRF scanning of cultural relics with irregular surfaces, obtaining detailed elemental distribution images. With the method we proposed, archaeologists will be able to perform large-area XRF scanning imaging on relics with irregular surfaces, rather than being limited to flat-surface scans. This innovation significantly extends the application scope of μXRF for large-area scanning and is poised to achieve more breakthroughs in archaeology.

The elemental information contained in cultural relics is essential to archaeologists. By acquiring elemental information from the surfaces of objects, archaeologists can better study and preserve cultural relics. They can employ different treatment methods based on the varying elemental composition of relics. The distribution of elements can also help archaeologists identify the authenticity of relics, as counterfeit items typically exhibit different types and distributions of elements compared to genuine ones. In addition, elemental information can reveal more potential value of cultural relics, and assist in archaeological research from various perspectives[1–3].

X-ray fluorescence (XRF) is a commonly used method for obtaining surface elemental information of objects. It is a non-destructive technique capable of performing rapid elemental analysis. Energy-dispersive XRF (EDXRF) is a widely utilized type of XRF in archaeology. By analyzing the energy of the peaks in the spectrum, it enables rapid identification and quantification of elements. In addition, XRF equipment is also characterized by miniaturization. Therefore, portable XRF is often used by archaeologists for in situ XRF elemental analysis[4].

μXRF is a variant of XRF technique and can analyze the elemental distribution characteristics in sample surfaces with high spatial resolution[5–9]. It uses a poly-capillary X-ray lens to focus X-rays into a micrometer-scale spot on the object's surface[10,11]. Therefore, μXRF can easily enhance the detector's count and achieve higher resolution, making it more advantageous in analyzing cultural relics with intricate structures.

Macro-XRF (MA-XRF) is a technique that utilizes XRF equipment for large-area elemental analysis, further extending the application range of XRF[12]. Scanning extensive surfaces can rapidly obtain elemental distribution images. Using μXRF equipment for MA-XRF scanning and imaging has become a growing trend in archaeology[13,14]. The scanning and imaging of paintings is an important application of MA-XRF. By performing large-area scans and analyses of paintings, it is possible to determine the composition of pigments and reveal hidden information such as underdrawings and the creative process[15–21]. Although time may cause physical or chemical changes to some relics, elemental information always remains on their surfaces. For faded or damaged relics, the elemental information obtained through MA-XRF scanning can effectively aid in analysis and restoration[22,23]. In addition, MA-XRF is playing a role in archaeology in other ways and has made unexpected achievements. M. Hložek et al. used μXRF to perform MA-XRF scanning on Roman-period enamel paint, describing the less-known technique of combining enamel with millefiori[24]. Gerken et al. combined μXRF scanning with LED-excited IRR and successfully visualized iron gall ink underdrawings, which is classified as an exceptional underdrawing material for paintings[25]. Capobianco et al. found traces of gold in two metal objects

[1]Institute of High Energy Physics, Chinese Academy of Sciences, Beijing, 100049, China. [2]Jinan Laboratory of Applied Nuclear Science, Jinan, 251401, China. [3]School of Nuclear Science and Technology, University of Chinese Academy of Sciences, Beijing, 100049, China. [4]Conservation Standards Research Institute, The Palace Museum, Beijing, 100009, China. [5]Institute of Archaeology, Chinese Academy of Social Sciences, Beijing, 100101, China. ✉e-mail: weicf@ihep.ac.cn; quliang@dpm.org.cn

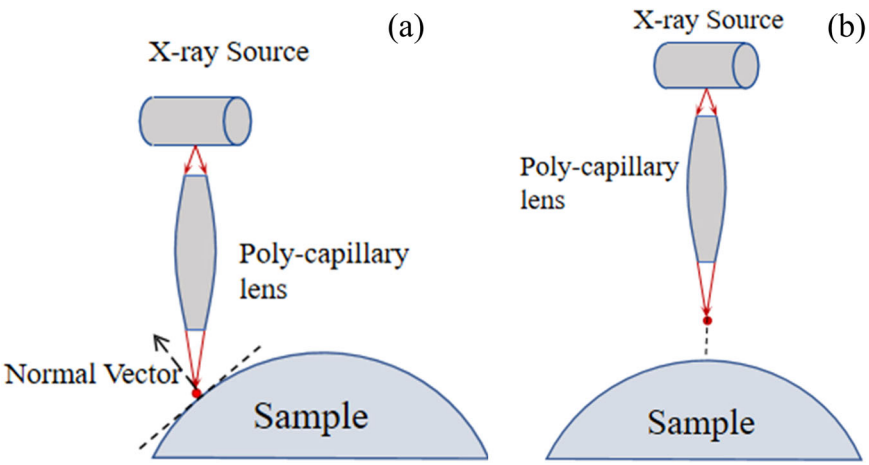

Fig. 1 | Geometric schematic of μXRF scanning on irregular surfaces. When scanning cultural relics with irregular surfaces, **a** changes in angle of incident X-rays and **b** changes in distance of incident X-rays.

from the archaeological site of Ferento, using μXRF mapping that suggested the precious character of these pieces[26]. Saverwyns et al. demonstrated the use of MA-XRF in studying the authenticity of paintings[27]. These studies utilized μXRF for large-area scanning and imaging, obtaining the distribution images of elements in the surface of cultural relics, successfully demonstrating the potential of μXRF in archaeological research.

For the current stage of archaeological research, a μXRF imaging system capable of 2D movement can cover most 2D flat scanning requirements[28–30]. The 2D translation stage can carry the μXRF system to perform large-area and rapid scanning on flat surfaces. Furthermore, some systems replace the 2D translation stage with a 3D translation stage[31]. Typically, these systems use distance-measuring devices to determine the position of the object surfaces, enabling more precise alignment of the μXRF system's working plane. However, the surfaces of actual relics are not always flat, posing challenges for large-area scanning and imaging. L. Cheng et al. placed small samples on a rotatable XYZ-θ stage, allowing the adjustment of the X-ray incident direction by changing the stage's angle[32]. For large and immovable relics, Hocquet et al. mounted the μXRF system on a remotely controlled 3D motion device. This allows the μXRF system to be rotated to look up or down[33]. This capability facilitates precise μXRF analysis of immovable curved objects. Furthermore, Ruvalcaba Sil et al. mounted the μXRF system on an articulating arm boom stand, allowing for manual rotation of the μXRF system at any angle[34]. Vavrik et al. combined XRF and CT into a single system. This system employs a rotation stage to perform 2D XRF mapping from multiple angles of the relics and integrates the XRF mapping results onto the 3D contour images obtained by CT[35]. Although μXRF analysis can be performed on curved relics, there are still challenges to curved μXRF scanning. The inability to capture the surface contours and the lack of a motion system that can automatically adjust based on the object's surface prevent the realization of surface adaptive μXRF scanning.

We previously developed a surface adaptive μXRF scanner, capable of performing μXRF imaging on objects with irregular surfaces[36]. A depth camera and a robotic arm are integrated into the basic μXRF system. The depth camera captures the surface contours of the cultural relic in the form of a 3D point cloud. The six-axis robotic arm can automatically move to designated scanning points and adjust the angle of the incident X-rays to remain perpendicular to the object's surface, based on the surface contour data processed by the algorithm. These make large-area MA-XRF scanning of curved cultural relics achievable. In previous experiments, we conducted several quantitative tests on the μXRF scanner, and the results demonstrated that the data obtained from curved surface scans are reliable and accurate. Additionally, the μXRF scanner has been successfully applied to ceramics, cylinders, stones, and other irregularly shaped objects, demonstrating its capability for adaptive scanning of curved surfaces. Through this method, the important surface analysis technique of large-area XRF scanning imaging can be successfully applied to relics with irregular surfaces. It provides archaeologists with a novel and powerful tool for analyzing elemental distributions on irregular relic surfaces.

In this paper, we further applied μXRF to cultural relics with irregular surfaces, demonstrating its significant potential in archaeology. We will first introduce the devices of the μXRF scanner, followed by presenting and discussing the μXRF imaging experiments of cultural relics with irregular surfaces.

Methods

Surface Adaptive μXRF Scanner

When scanning cultural relics utilized μXRF systems, in order to ensure the accuracy of the elemental distribution, the incident X-rays should be perpendicular to the surface of the object and the distance from the X-ray lens to the surface of the object should be constant. However, when scanning cultural relics with irregular surfaces, as shown in Fig. 1, the incident angle and distance of the X-rays will vary with the inclination of the surface. This can significantly affect the accuracy of detector counting and elemental analysis.

To eliminate the errors, we use a surface adaptive μXRF device equipped with a depth camera and a robotic arm as shown in Fig. 2. The depth camera accurately measures and calculates the surface contours and normal vectors of the objects. And the robotic arm can carry the spectrometer and perform both translation and rotation, ensuring that the incident X-ray is maintained perpendicular to the object's surface and the μXRF spectrometer works at a constant distance from the sample surface. This configuration allows us to obtain surface contours and scan from any angle without changing the position of the object. As a result, the surface adaptive μXRF scanner is capable of performing μXRF mapping on cultural relics with arbitrary irregular surfaces. In addition, the scanning radius of the robotic arm is more than 900 mm, and motion accuracy is less than 30 μm, which allows the system to complete large-area scans.

The imaging system devices are installed within a black protective housing as shown in Fig. 2 and are mounted on a robotic arm. The target of the X-ray source is a Mo target, with the energy of characteristic X-ray being 17.4 keV. The poly-capillary lens designed for the Mo target converges the X-rays into a focal spot, that remains on the surface of the object during scanning. When the energy of the incident X-ray is 17.4 keV, its back focal length is 17.8 mm, where the focal spot size is 42.2μm. The SDD offers an energy resolution better than 129 eV. In addition to the μXRF spectrometer, the laser helps visualize the focal spot.

Workflow

When starting to scan a cultural relic, it is first placed in an appropriate position and orientation. The depth camera captures the 3D contour of the

Fig. 2 | Surface adaptive μXRF scanner based on robotic arm.

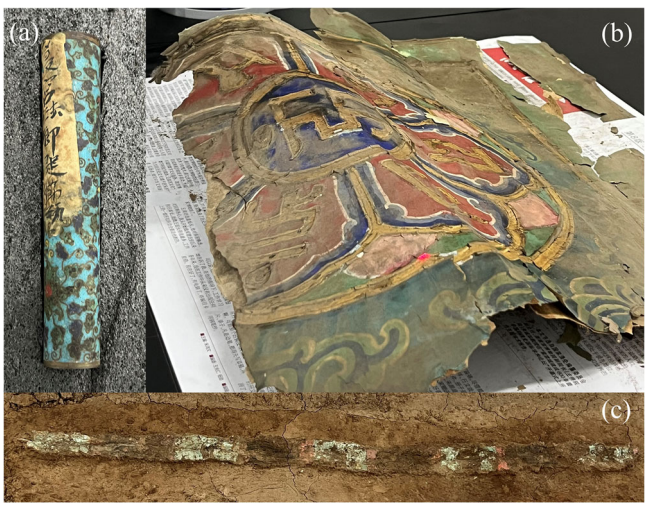

Fig. 3 | Cultural relics with irregular surfaces. a An enamel cylinder covered with paper, (**b**) a fallen painting from the ancient architecture retains its curved shape, and (**c**) a decayed wooden gnomon shadow template.

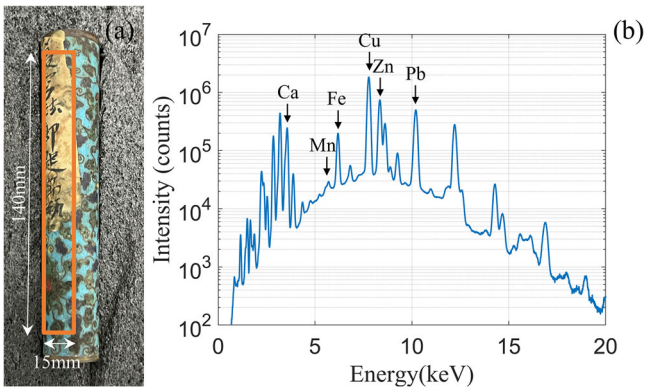

Fig. 4 | The enamel cylinder covered with paper and its spectral analysis results. a ROI of the enamel cylinder. **b** Elements present in the enamel cylinder. Unless otherwise specified, the characteristic X-ray peaks of the elements labeled in this article correspond to their K-α X-ray lines. The L-α X-ray line of Pb is labeled here.

object. After processing through our developed software, the contour can be converted into a path executable by the robotic arm. Subsequently, the robotic arm carries the μXRF spectrometer and performs scanning at each scan point. Since the path information includes the 3D coordinates and normal vectors of each scan point, the robotic arm can ensure that the incident X-rays maintain perpendicular to the object's surface throughout the scanning process. During the entire scanning process, the time taken to move from one scanning point to the next primarily consists of translation time and rotation time. For areas with significant angle changes, the robotic arm's rotation consumes more time. However, for areas with smooth and continuous angle changes, the rotation time of the robotic arm can be considered negligible. However, it is worth noting that for a curved object, surface-adaptive scanning will cover a larger area than planar scanning. For example, in the case of a hemispherical object with a radius r, a flat scan would cover an area of πr^2. In contrast, surface-adaptive scanning would cover an area of $2\pi r^2$. Since its surface normal varies continuously, the time required for the robotic arm to adjust its orientation can be considered negligible. Therefore, the overall time cost of surface-adaptive scanning is approximately twice that of flat scanning.

After the scanning is completed, our developed software automatically analyzes the elements present in the object's surface and generates surface elemental distribution images for each element in the form of a 3D point cloud. If the cultural relic cannot be scanned in a single session, the above steps need to be repeated. The scanning results are then stitched together to form a complete surface elemental distribution image.

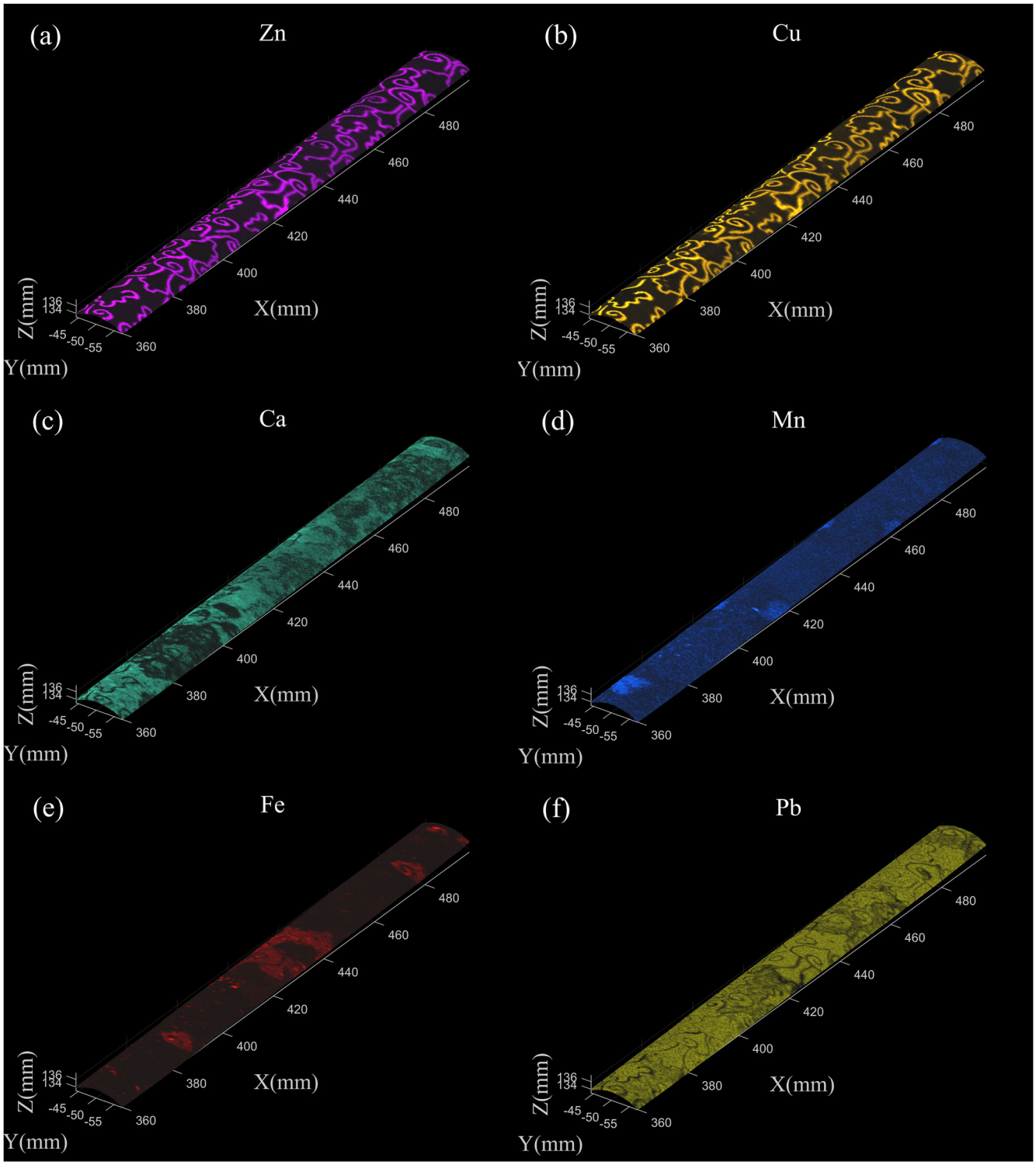

Fig. 5 | Surface elemental distribution images of the enamel cylinder. (**a**) Zn, (**b**) Cu, (**c**) Ca, (**d**) Mn, (**e**) Fe, and (**f**) Pb.

Materials

The elemental distribution in the surfaces of cultural relics is crucial information for archaeologists. Obtaining the surface elemental distribution of cultural relics with irregular surfaces is our primary concern. The surface adaptive μXRF scanner enables large-area, high-precision scanning of most cultural relics with irregular surfaces. To demonstrate this capability, we present scanning experiments on three representative cultural relics.

The enamel cylinder present in Fig. 3a is a Ming Dynasty cloisonne enamel from the Palace Museum. Decades ago, due to human intervention, it was covered with paper and glue. When the researchers attempted to re-study the enamel cylinder, they found that some of the paper had become difficult to remove. To avoid damaging the relic during research, we conducted a curved surface μXRF scan on it using the surface adaptive μXRF scanner.

The fallen painting from the ancient architecture, shown in Fig. 3b is also from the Palace Museum and its area is approximately 530 mm × 330 mm.

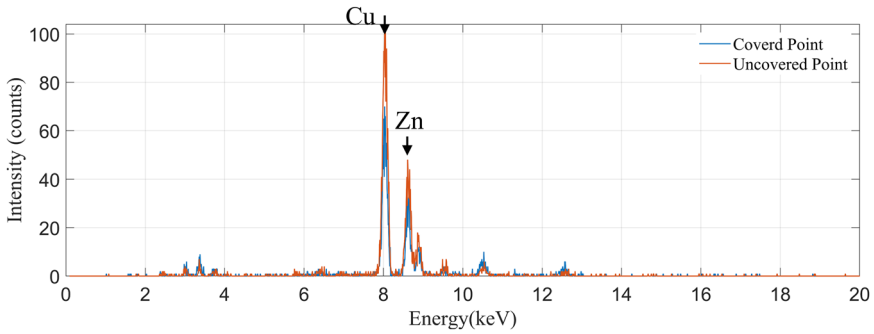

Fig. 6 | The comparison of the spectra from points on the metal contour covered by paper and those uncovered.

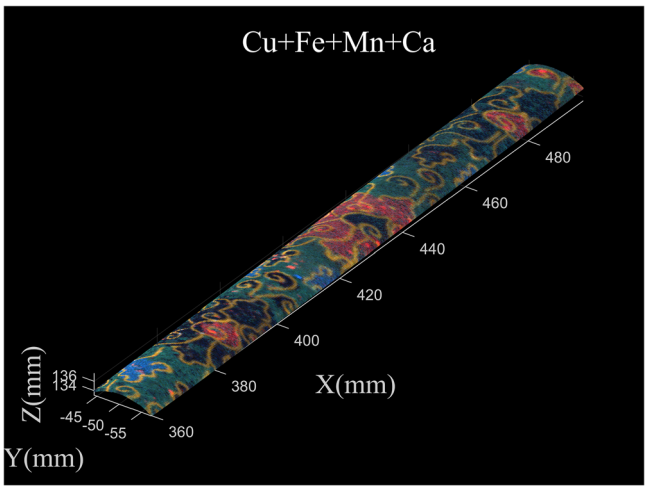

Fig. 7 | The fused image of Cu, Fe, Mn, and Ca.

This painting was originally painted on a column of the architecture in the Forbidden City during the Qing Dynasty. Due to the passage of time, the surface of the architecture has undergone falling and flaking. Researchers obtained a part of the painting from the ancient architecture to study the distribution of elements. However, this part of the painting retains its curved shape, making it unsuitable for flat μXRF scanning. To detect the distribution of elements in the surface of the fallen painting, we used the surface adaptive μXRF scanner to perform a μXRF imaging of the fallen painting.

The gnomon shadow template is an ancient Chinese tool used for measuring time[37]. Ancient people placed a wooden pole vertically on the ground, and at a fixed time each day, they would use another pole with patterns to measure the length of the shadow to determine the corresponding date. In the Northern Hemisphere, the shadow of a wooden pole is the shortest during the summer solstice and the longest during the winter solstice. This gnomon shadow template excavated from the Taosi site in Shanxi is a painted wooden pole with a history of over 4,000 years[38]. As shown in Fig. 3c, the red and green pigments on the gnomon shadow template are distributed segmentally and follow a regular pattern. Archaeologists speculate that the patterns on the wooden pole were used as scales for measuring the length of shadows[39]. At a fixed time each day, the length of the shadow cast by a vertically placed wooden rod changes regularly throughout the year. It can be inferred that each section of pigment on the horizontal gnomon shadow template corresponds to a specific date in the year. Therefore, μXRF scanning can accurately determine the types and distributions of elements in the surface of the gnomon shadow template. Additionally, identifying the elemental composition of the pigments is essential for inferring the specific period in which the gnomon shadow template was used. Unfortunately, its wooden structure has severely decayed, and some of the paint has become blurred and indistinct.

Results

the Enamel Cylinder Covered with Paper

Figure. 4a shows the scanned area of the enamel cylinder, with a scanning area of approximately 140 mm × 15 mm. The scanning was performed at 30 kV/0.5 mA, with a spatial resolution (scanning point interval) of 150 μm and a dwell time of 0.2 s per point. The total scanning time is 4 h 10 min.

As shown in Fig. 4b, Zn, Pb, Mn, Fe, Cu, and Ca were detected and surface elemental distribution images were generated in Fig. 5. From the 3D point cloud, it can be observed that the height variation in the scanned area is approximately 4 mm. In addition, it is easy to find that Zn and Cu are mainly distributed in the metal contours of the patterns. Fe is distributed in the red pigment, and Mn is also present in some violet areas. Ca and Pb are components of the background material of the enamel tube. As shown in Fig. 5, Ca and Pb are distributed across most areas, and their counts may be influenced by the distribution of other elements on the enamel cylinder's surface.

To figure out the impact of the covering paper on the detector counts, we present in Fig. 6 the spectra of the point in the metal contour covered by paper and the uncovered metal contour. Since the metal contour primarily contains Cu and Zn, these two spectra are presented without the logarithmic scale to better visualize the differences between the peaks of the covered point and the uncovered point. The results show that the Cu counts in the metal contour covered by paper are about 33% lower than those in the uncovered metal contour. This demonstrates that the scanning results are reasonable and reliable, and the detector's counts are sufficient to distinguish the patterns covered by the paper.

The fused image of four elements is shown in Fig. 7, revealing the pattern that should be displayed on the surface of the enamel cylinder beneath the paper, as well as the distribution of each element. This indicates that the surface adaptive μXRF scanner can reveal patterns beneath the covering without causing damage to the relics, provided the covering is sufficiently thin and the absorption of the emitted characteristic X-rays is limited.

The Fallen Painting from Ancient Architecture

The entire relic is predominantly convex, and can be entirely scanned using the μXRF scanner. However, to prevent excessive time consumption, the resolution would need to be reduced when scanning the entire relic. To obtain more representative scanning results with higher resolution, we selected the convex areas with the most significant height variation for scanning. As shown in Fig. 8a, the ROI of the fallen painting is approximately 135 mm × 110 mm. The experiment was conducted under 30 kV/0.5 mA conditions, with a spatial resolution of 400 μm and a dwell time of 0.1 s per point. The total scanning time is 2 h 17 min.

The elements present in the surface of the fallen painting are marked in Fig. 8b and surface elemental distribution images are shown in Fig. 9. At the same time, as shown in Fig. 10, we also analyzed the Raman spectra of the red and blue pigments using the inVia 2000 confocal Raman microscope (Renishaw) with a 532 nm laser. It is obvious that the distributions of Hg and As coincide with the distribution of the red pigment, and S is

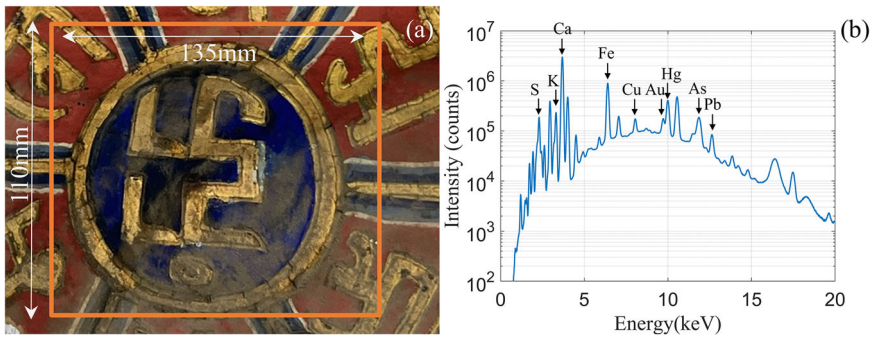

Fig. 8 | The fallen painting from ancient architecture and its spectral analysis results. a The top view of the ROI of the fallen painting from ancient architecture, and (**b**) elements present in the fallen painting. Due to the proximity of the energy of the K-α line of As and the L-α line of Pb, we have labeled the K-β line of As and the L-β line of Pb in the figure. The L-α line of Au is also labeled here.

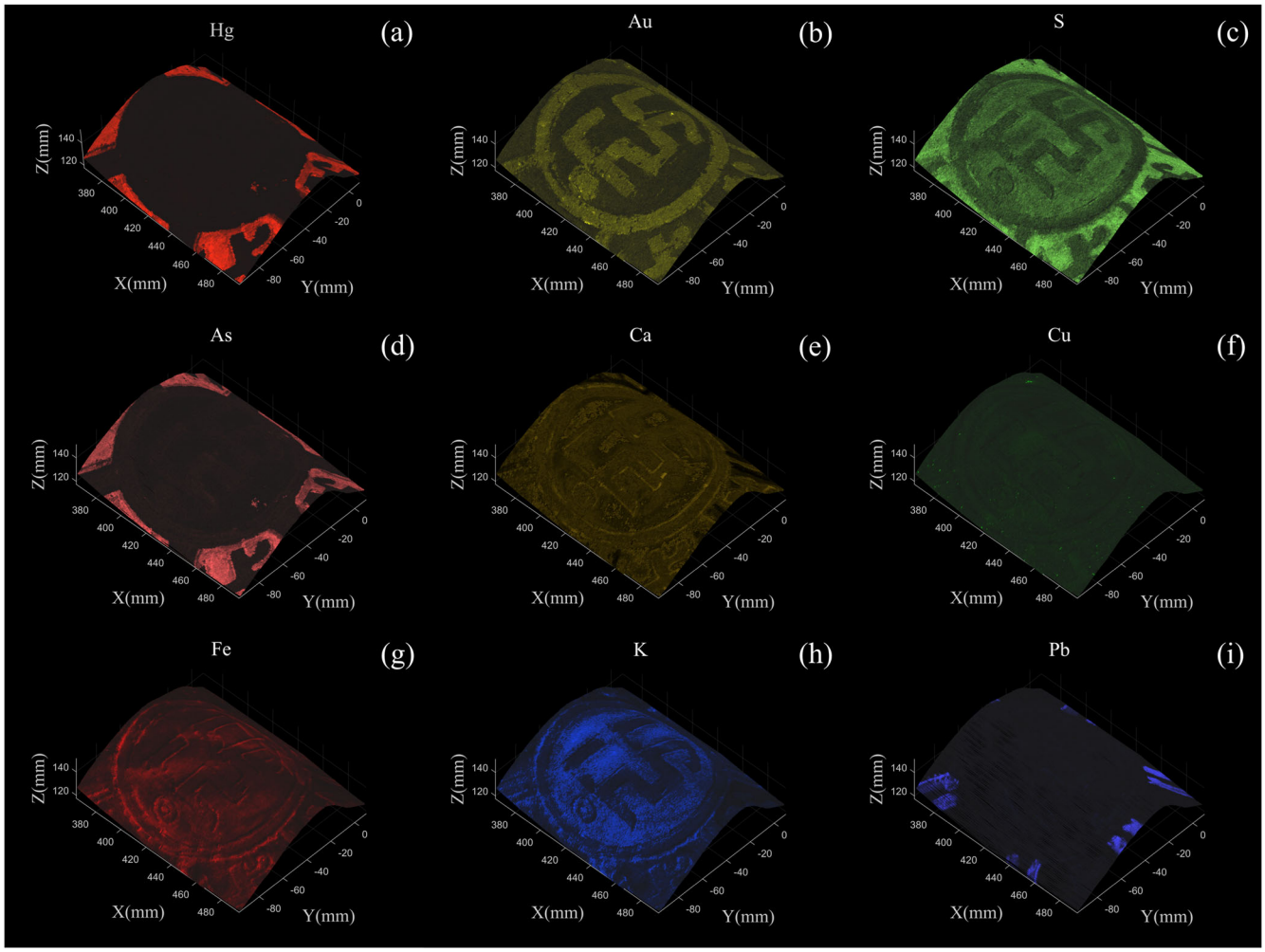

Fig. 9 | Surface elemental distribution images of the fallen painting from ancient architecture. (**a**) Hg, (**b**) Au, (**c**) S, (**d**) As, (**e**) Ca, (**f**) Cu, (**g**) Fe, (**h**) K and (**i**) Pb.

also present in the region of red pigment. In the Raman spectroscopy results shown in Fig. 10a, only the characteristic peaks of HgS were detected. Therefore, we conclude that the red pigment is cinnabar, while As is present in other layers, with its distribution merely coinciding with that of the red pigment. From the Raman spectroscopy results in Fig. 10b, we observed that the Raman spectrum of the blue pigment matches the characteristics of ultramarine. The 544 cm^{-1} peak is typically associated with the sulfide component in ultramarine and the 1093 cm^{-1} peak is related to the silicate structure of ultramarine. Based on these two characteristic peaks, we can clearly identify the blue pigment as ultramarine. Among the elements shown in Fig. 9, only S is present in ultramarine, which explains why S is also distributed in the blue pigment region in Fig. 9c. Only the distribution of Au matches that of the gold pigment, allowing us to infer that the gold pigment is a compound containing Au. Thus, we have analyzed the composition and elemental distribution of three pigments. As for the remaining elements—K, Ca, Fe, Cu, As, and Pb—we consider them to be present in other layers, such as background materials or impurities in pigments. The fusion image of Au

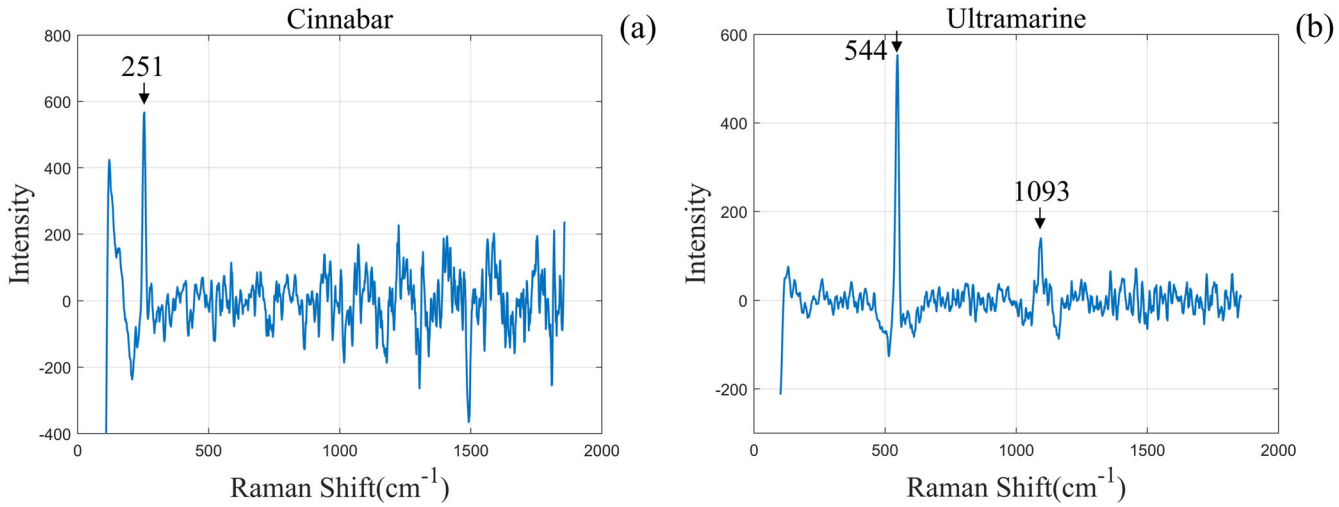

Fig. 10 | The Raman spectra results of the fallen painting from ancient architecture. a The red pigment (cinnabar) and (**b**) the blue pigment (ultramarine).

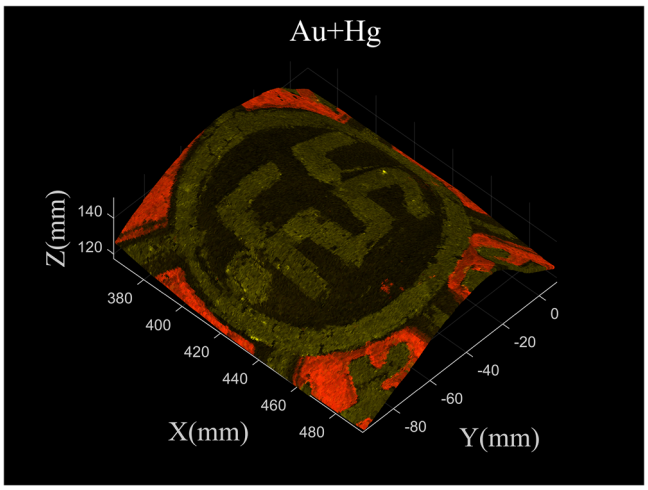

Fig. 11 | The fused image of Hg and Au.

and Hg is shown in Fig. 11, which effectively reproduces the element through the scanning and shape characteristics of the fallen painting. Besides the elemental information, Fig. 9 also reveals that the height variation in the scanned area is approximately 30 mm.

In addition to this experiment, many similar paintings, after long-term preservation, have suffered from fading and falling. However, the elements in the surface of the relics remain preserved. To obtain the elemental distribution in the surface of the paintings, MA-XRF is essential. In many architectures in the field of cultural heritage, many paintings were created on curved surfaces such as ceilings, columns, and arches[40]. Conventional MA-XRF systems are unable to perform adaptive scanning on curved surfaces. Therefore, the surface adaptive μXRF scanner is particularly crucial in addressing this challenge.

The Gnomon Shadow Template

As shown in Fig. 12a, to avoid damaging the gnomon shadow template, we kept it in its original wooden box and used the surface adaptive μXRF scanner to perform a in situ large-area μXRF scan of its surface. Figure. 13a shows the top view of the scanning region and the scanned area is 660 mm × 50 mm. The experiment was performed at 30 kV/0.5 mA, with a spatial resolution (scanning point interval) of 400 μm and a dwell time of 0.1 s per point. The total scanning time is 6 h 28 min.

The results in Fig. 12b showed that the surface of the gnomon shadow template primarily contains Cu and Hg in the paint. The green pigment is primarily composed of Cu, while the red pigment is mainly composed of Hg. Fe and Ca are elements found in the soil and wood, respectively. The elemental distribution images of the scanning region are displayed separately in Fig. 13. It can be observed that the height variation in the scanned area is approximately 60 mm. The elemental distribution images of Cu and Hg can restore the original distribution of the pigments. By combining the images of Cu and Hg, we can accurately determine the positions of the markings made by ancient humans on the wooden pole to measure the sun's shadow.

The red pigment contains Hg, and the green pigment contains Cu, which are entirely consistent with the painting techniques and characteristics of other lacquerware relics unearthed from the same region[38]. Based on the information provided by these lacquerware relics, it can be inferred that the gnomon shadow template was created and used around 2,000 BCE, corresponding to the mid-to-late period of the Taosi culture.

Discussion

This study achieved large-area μXRF scanning of cultural relics with irregular surfaces, using a surface adaptive μXRF scanner. The surface adaptive μXRF scanner employs a robotic arm as the motion device, enabling it to adapt to cultural relics with various shapes and sizes flexibly.

From the above experiments, it can be concluded that the surface adaptive μXRF scanner can play a significant role in the study of cultural relics. For the enamel cylinder covered with paper, a large-area curved surface scanning successfully detected Zn, Pb, Mn, Fe, Cu, and Ca, and generated surface elemental distribution images of the area covered by the paper, bringing the hidden patterns back into view. For the fallen painting from ancient architecture, obtaining the elemental distribution on its surface is challenging, as most architectural surfaces are curved. We employed the surface adaptive μXRF scanner to obtain the elemental distribution in the surface of the fallen painting and generated surface distribution images of Hg and Au. A large-area μXRF scan was conducted on the gnomon shadow template from the Taosi site in Shanxi, which had suffered severe decay in its wooden structure. The results effectively demonstrated the surface elemental distribution of Cu and Hg in the surface of the cultural relic. In the above experiments, the surface adaptive μXRF scanner solved the problem that current μXRF systems cannot automatically obtain the contours of objects' surface and perform curved surface scans, and successfully acquired elemental information from curved surfaces. More importantly, different from traditional μXRF results presentation, this system displays the surface elemental distribution in the form of a 3D point cloud, which can accurately restore the distribution of elements in 3D space.

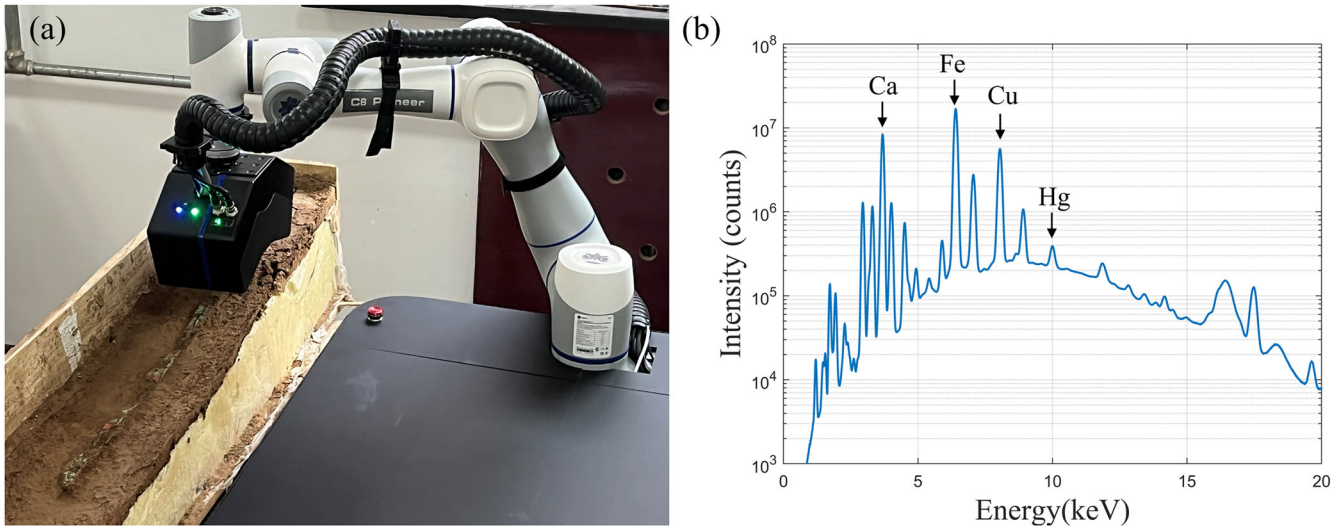

Fig. 12 | The gnomon shadow template and its spectral analysis results. a The scanning experiment of the gnomon shadow template. **b** Elements present in the gnomon shadow template.

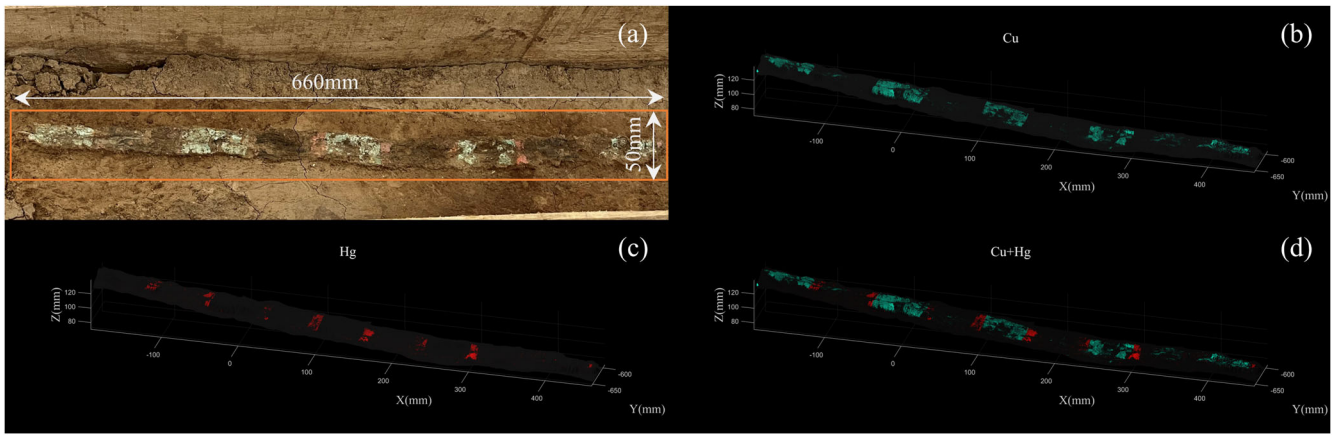

Fig. 13 | Scanning area and elemental distribution images of the gnomon shadow template. a The top view of the scanning region of the gnomon shadow template, and surface elemental distribution images of (**b**) Cu, (**c**) Hg, and (**d**) the fused image of these two elements.

However, although our scanner can perform scans of most curved surface, archaeologists are more concerned about the safety of cultural relics during the scanning process. The surface adaptive μXRF scanner offers comprehensive multi-faceted safety measures to address this concern. After the depth camera captures the contour information of the cultural relics, our developed algorithm evaluates the positions of the scanning points. Before the scanning begins, unsafe scanning points are eliminated. During the scanning process, the distance sensor continuously monitors for dangerously close distances, ensuring that the equipment halts operation promptly when necessary. All these measures ensure the safe execution of cultural relic scanning.

Although the surface adaptive μXRF scanner can perform μXRF scans on most cultural relics with irregular surfaces, it still has certain limitations. It is noticeable that, due to safety constraints, the oversized black protective housing prevents the scanning of certain recessed areas on objects with intricate structures. Specifically, while most convex areas of relics can be scanned, areas with excessive concavity pose a risk of collision between the relic and the protective housing. To prevent damage, the system promptly halts operation when the distance sensor detects that the protective housing is too close to the relic in some directions. Therefore, miniaturization of the equipment is crucial for scanning intricately structured relics. In addition, another critical research addressing this issue is the weighted correction of unscannable points. He et al. have developed relevant algorithms to perform planar scans on objects with irregular surface. Subsequently, they applied weighted corrections to detector counts based on the shape of object's surface, resulting in more accurate elemental distribution[41]. In future work, based on the existing surface adaptive μXRF scanner, we will further develop a weighted correction algorithm for detector counts with changing incident angles. This will enable more accurate corrections of detector counts during 3D curved surface scanning.

Another factor limiting the performance of the surface adaptive μXRF scanner is the fixation of the robotic arm on the object platform. For large cultural relics such as murals that do not require an object platform, we plan to develop a detachable μXRF scanner. The robotic arm can be freely moved on the ground, while its precise position in space will be accurately recorded. This will enable large-area μXRF scanning while the robotic arm is being moved.

XRF scanning imaging is an important method for archaeologists to study the elemental distribution on the surfaces of relics. However, existing techniques are unable to perform large-scale, precise scanning on relics with

irregular surfaces. The above discussion demonstrates that the surface adaptive μXRF scanner provides crucial support for element analysis of damaged or covered curved relics and elemental distinguishing and imaging of curved relics. The surface adaptive μXRF scanner addresses the issue that some cultural relics with complex surfaces cannot be scanned on a large scale using existing μXRF imaging systems. It innovatively provides a new elemental analysis approach for cultural relic research.

Data availability

The datasets generated and analysed during the current study are not publicly available, but are available from the corresponding author on reasonable request. The codes developed for this study are currently not publicly available, but are available from the corresponding author on reasonable request.

Received: 24 December 2024; Accepted: 3 July 2025;
Published online: 25 July 2025

References

1. Madariaga, J. M. Analytical chemistry in the field of cultural heritage. *Anal. Methods* **7**, 4848–4876 (2015).
2. Nevin, A., Spoto, G. & Anglos, D. Laser spectroscopies for elemental and molecular analysis in art and archaeology. *Appl. Phys. A* **106**, 339–361 (2012).
3. Szentmiklósi, L. et al. Integration of neutron-based elemental analysis and imaging methods and applications to cultural heritage research. *J. Archaeol. Sci. Rep.* **20**, 476–482 (2018).
4. Frahm, E. & Doonan, R. C. P. The technological versus methodological revolution of portable XRF in archaeology. *J. Archaeol. Sci.* **40**, 1425–1434 (2013).
5. Vicenzi, E. P. et al. Major to trace element imaging and analysis of iron age glasses using stage scanning in the analytical dual beam microscope (tandem). *Herit. Sci.* **10**, 90 (2022).
6. Bauer, L. J. et al. Chemical mapping of teeth in 2D and 3D: X-ray fluorescence reveals hidden details in dentine surrounding fillings. *Acta Biomater.***109**, 142–152 (2020).
7. Ramos, I. et al. Elemental mapping of biofortified wheat grains using micro X-ray fluorescence. *Spectrochimica Acta Part B: At. Spectrosc.* **120**, 30–36 (2016).
8. Wouters, B. et al. Characterization of archaeological metal remains in micromorphological thin sections using μXRF elemental mapping. *Geoarchaeology* **32**, 311–318 (2017).
9. Langstraat, K. et al. Large area imaging of forensic evidence with MA-XRF. *Sci. Rep.* **7**, 15056 (2017).
10. Schields, P. J. et al. Overview of polycapillary X-ray optics. *Powder Diffr.* **17**, 70–80 (2002).
11. Haschke, M. & Haller, M. Examination of poly-capillary lenses for their use in micro-XRF spectrometers. *X-Ray Spectrom. Int. J.* **32**, 239–247 (2003).
12. Janssens, K. et al. Use of microscopic XRF for non-destructive analysis in art and archaeometry. *X-Ray Spectrom.* **29**, 73–91 (2000).
13. Legrand, S. et al. MA-XRF imaging as a tool to characterize the 16th century heraldic stained-glass panels in Ghent Saint Bavo Cathedral. *J. Cultural Herit.* **40**, 163–168 (2019).
14. Magkanas, G. et al. Illuminated manuscript analysis methodology using MA-XRF and NMF: Application on the Liber Feudorum Maior. *Microchem. J.* **165**, 106112 (2021).
15. Delaney, J. K. et al. Integrated X-ray fluorescence and diffuse visible-to-near-infrared reflectance scanner for standoff elemental and molecular spectroscopic imaging of paints and works on paper. *Herit. Sci.* **6**, 1–12 (2018).
16. Turner, N. K. et al. Visualizing underdrawings in medieval manuscript illuminations with macro-X-ray fluorescence scanning. *X-Ray Spectrom.* **48**, 251–261 (2019).
17. Mazzinghi, A. et al. The importance of being little: MA-XRF on manuscripts on a Venetian island. *X-Ray Spectrom.* **50**, 272–278 (2021).
18. Alfeld, M. et al. A mobile instrument for in situ scanning macro-XRF investigation of historical paintings. *J. Anal. At. Spectrom.* **28**, 760–767 (2013).
19. Legrand, S. et al. Examination of historical paintings by state-of-the-art hyperspectral imaging methods: from scanning infra-red spectroscopy to computed X-ray laminography. *Herit. Sci.* **2**, 1–11 (2014).
20. Alfeld, M. et al. Optimization of mobile scanning macro-XRF systems for the in situ investigation of historical paintings. *J. Anal. At. Spectrom.* **26**, 899–909 (2011).
21. Debastiani, R. et al. Identification of green pigments from fragments of Roman mural paintings of three Roman sites from north of Germania Superior. *Appl. Phys. A* **122**, 1–12 (2016).
22. Radepont, M. et al. Revealing lost 16th-century royal emblems on two Andrea Amati's violins using XRF scanning. *Herit. Sci.* **8**, 1–12 (2020).
23. Ricciardi, P. et al. Macro X-ray fluorescence (MA-XRF) scanning of illuminated manuscript fragments: potentialities and challenges. *Microchem. J.* **124**, 785–791 (2016).
24. Hložek, M. et al. Enamel paint techniques in archaeology and their identification using XRF and micro-XRF. *Radiat. Phys. Chem.* **137**, 243–247 (2017).
25. Gerken, M., Sander, J. & Krekel, C. Visualising iron gall ink underdrawings in sixteenth century paintings in-situ by micro-XRF scanning (MA-XRF) and LED-excited IRR (LEDE-IRR). *Herit. Sci.* **10**, 78 (2022).
26. Capobianco, G. et al. μXRF mapping as a powerful technique for investigating metal objects from the archaeological site of Ferento (Central Italy). *J. Imaging* **6**, 59 (2020).
27. Saverwyns, S., Currie, C. & Lamas-Delgado, E. Macro X-ray fluorescence scanning (MA-XRF) as tool in the authentication of paintings. *Microchem. J.* **137**, 139–147 (2018).
28. Hocquet, F. P. et al. Elemental 2D imaging of paintings with a mobile EDXRF system. *Anal. Bioanal. Chem.* **399**, 3109–3116 (2011).
29. Romano, F. P. et al. Real-time elemental imaging of large dimension paintings with a novel mobile macro X-ray fluorescence (MA-XRF) scanning technique. *J. Anal. At. Spectrom.* **32**, 773–781 (2017).
30. Alberti, R. et al. CRONO: a fast and reconfigurable macro X-ray fluorescence scanner for in-situ investigations of polychrome surfaces. *X-Ray Spectrom.* **46**, 297–302 (2017).
31. Pouyet, E. et al. Development of a highly mobile and versatile large MA-XRF scanner for in situ analyses of painted work of arts. *X-Ray Spectrom.* **50**, 263–271 (2021).
32. Cheng, L. et al. Development of a micro-X-ray fluorescence system based on polycapillary X-ray optics for non-destructive analysis of archaeological objects. *Spectrochim. Acta Part B: At. Spectrosc.* **62**, 817–823 (2007).
33. Hocquet, F. P. et al. A remote controlled XRF system for field analysis of cultural heritage objects. *X-Ray Spectrom. Int. J.* **37**, 304–308 (2008).
34. Ruvalcaba Sil, J. L. et al. SANDRA: a portable XRF system for the study of Mexican cultural heritage. *X-Ray Spectrom.* **39**, 338–345 (2010).
35. Vavřík, D. et al. Analysis of baroque sculpture based on X-ray fluorescence imaging and X-ray computed tomography data fusion.*7th Conference on industrial computed tomography*, Leuven, Belgium 7–9 (2017).
36. Wang, Y. et al. Three-dimensional μXRF imaging system for curved surface. *IEEE Trans. Instrum. Meas.* **73**, 1–11 (2024).
37. He, N. On the gnomon shadow template function of the lacquer stick from the royal Tomb IIM22 at Taosi walled-town of middle period. *Stud. Hist. Nat. Sci.* **28**, 261–276 (2009).
38. He, N. Taosi: an archaeological example of urbanization as a political center in prehistoric China. *Archaeol. Res. Asia* **14**, 20–32 (2018).
39. He, N. Supplementary research on the Gnomon shadow template from Taosi. *Stud. Hist. Nat. Sci.* **30**, 278–287 (2011).

40. Carpiceci, M. Survey problems and representation of architectural painted surfaces. *Int. Arch. Photogramm. Remote Sens. Spat. Inf. Sci.* **38**, 523–528 (2012).
41. He, Z. et al. Improving spatial resolution and correcting surface topography in portable macro-XRF imaging devices. *IEEE Trans. Nucl. Sci.* **71**, 2151–2161 (2024).

Acknowledgements

The Key Scientific Research Base of Nuclear Technology Application and Equipment in the Field of Cultural Heritage (Institute of High Energy Physics, CAS), National Cultural Heritage Administration and "Archaeological Talent Promotion Program of China" (No: 2024-281).

Author contributions

C.W., Q.X., Y.W., L.W. developed the surface adaptive uXRF; Q.X., Y.W., X.Z., P.D., L.Q. wrote the main manuscript; L.Q., Q.X., Y.W., X.Z., P.D. did the experiments in Section the Enamel Cylinder Covered with Paper and the Fallen Painting from Ancient Architecture; Q.X., Y.W., X.Z., Y.L., J.G. did the experiment in Section the Gnomon Shadow Template.

Competing interests

The authors declare no competing interests.

Additional information

Correspondence and requests for materials should be addressed to Cunfeng Wei or Liang Qu.